Article

Phenylthiomethyl ketone-based fragments show selective and irreversible inhibition of enteroviral 3C proteases

Robert Schulz, Amira Atef, Daniel Becker, Franziska Gottschalk, Carolin Tauber, Stefan Wagner, Christoph Arkona, Atef A Abdel-Hafez, Hassan H Farag, Jörg Rademann, and Gerhard Wolber

J. Med. Chem., **Just Accepted Manuscript** • DOI: 10.1021/acs.jmedchem.7b01440 • Publication Date (Web): 12 Jan 2018

Phenylthiomethyl ketone-based fragments show selective and irreversible inhibition of enteroviral 3C proteases

Robert Schulz,[†] *Amira Atef,*[‡] *Daniel Becker,*[†] *Franziska Gottschalk,*[†] *Carolin Tauber,*[†] *Stefan Wagner,*[†] *Christoph Arkona,*[†] *Atef A. Abdel-Hafez,*[‡] *Hassan H. Farag,*[‡] *Jörg Rademann,*[†] *Gerhard Wolber**[†]

[†] Pharmaceutical and Medicinal Chemistry, Institute of Pharmacy, Freie Universität Berlin, Königin-Luise Straße 2+4, 14195

[‡] Medicinal Chemistry Department, Faculty of Pharmacy, Assiut University, Assiut 71526, Egypt

Abstract

Lead structure discovery mainly focuses on the identification of noncovalently binding ligands. Covalent linkage, however, is an essential binding mechanism for a multitude of successfully marketed drugs although discovered by serendipity in most cases. We present a concept for the *design* of fragments covalently binding to proteases. Covalent linkage enables fragment binding unrelated to affinity to shallow protein binding sites and at the same time allows differentiated targeted hit verification and binding location verification through mass spectrometry. We describe a systematic and rational computational approach for the identification of covalently

binding fragments from compound collections inhibiting enteroviral 3C protease, a target with high therapeutic potential. By implementing reactive groups potentially forming covalent bonds as chemical feature in our 3D pharmacophore methodology, covalent binders were discovered by high-throughput virtual screening. We present careful experimental validation of the virtual hits using enzymatic assays and mass spectrometry unraveling a novel, previously unknown irreversible inhibition of the 3C protease by phenylthiomethyl ketone-based fragments. Subsequent synthetic optimization through fragment growing and reactivity analysis against catalytic and non-catalytic cysteines revealed specific irreversible 3C protease inhibition.

Introduction

The group of covalently binding drugs comprises several prominent and relevant members such as acetylsalicylic acid, β-lactam antibiotics, proton-pump inhibitors like omeprazole or the antiplatelet agent clopidogrel, one of the best-selling drugs.[1-4] Covalent binding, however, is rarely considered in drug-design as a general reluctance resides in the pharmaceutical industry due to the putative risk of adverse drug reactions.[5] This bias changed recently as described by the title of a review by Singh *et al*. entitled "The resurgence of covalent drugs".[6] Covalent linkage is not only associated with risks, but also with advantageous target binding characteristics: (i) prolonged target interaction, (ii) increased binding affinity, (iii) pharmacokinetic and pharmacodynamic decoupling and (iv) improved selectivity.[7-12] In combination with fragment-based approaches, covalent binding has been utilized (i) for the identification of starting points for inhibitor design, (ii) exploration of novel binding sites on proteins or (iii) assessing ligandability of proteins.[13-16] Covalent bond formation enables fragment binding unrelated to affinity at shallow protein sites and hit identification and verification through mass spectrometry.

Existing approaches utilize covalent fragments (i) from accessible compound collection through substructure filters, (ii) chemical synthesis of probes or entire molecule collections or (iii) virtual libraries build from commercially available synthetic precursors with subsequent synthesis of virtual screening hits.[12, 14, 15, 17]. Recently, we have applied protein-templated fragment ligation as an approach for the discovery of irreversible protease inhibitors. [15 18]

Irreversible protein binding consists of the initial formation of a reversible non-covalent complex EI, which subsequently undergoes transition to the final complex E-I through covalent bond formation. The potency of such an inhibitor is given by the second order rate constant k_{inact}/K_I [$M^{-1}s^{-1}$]. Thereby, k_{inact} denotes the rate of covalent bond formation, whereas K_I accounts for the stability of the initial complex due to the formation of favorable non-covalent interactions as represented by the following scheme:

$$E + I \underset{K_I}{\rightleftharpoons} EI \xrightarrow{k_{inact}} E\text{-}I$$

.

In order to identify covalent fragments, whose binding is driven by K_I rather than k_{inact}, Kathmann *et al*. proposed to only use covalent fragments with identical warheads, where the reactivity is merely depending on substitution effects. This way, the best hits result from the formation of favorable non-covalent interactions.[17] Thereby, the pointless investigation of the most-active hits that are only driven by the reactivity of the warhead is circumvented. However, this approach can only be applied when working in a limited chemical space: Warhead types and the addressed target as initial knowledge about applicable covalent interactions are a prerequisite. Furthermore, synthesis efforts prior to the fragment screening are necessary.

Here we report a rational, computer-driven approach for the selection of covalently binding fragments from tangible as well as virtual molecule sources using 3D pharmacophores. Through

the introduction of a novel covalent bond feature type, a 3D pharmacophore captures the formation of the essential non-covalent interaction as well as the necessary spatial orientation of the warhead moiety for the subsequent covalent binding. This was utilized for identification of covalently binding fragments for 3C protease ($3C^{pro}$), which is essential for the replication of clinically relevant and emerging enteroviruses such as the coxsackievirus B3 (CVB3) being associated with (i) aseptic meningitis, (ii) cardiomyopathy, (iii) type-1 diabetes and (iv) most recently with dementia.[19-22] Therefore, $3C^{pro}$ has been indicated as a promising target for the design of enterovirus inhibitors for which the shallow polyprotein binding $3C^{pro}$ active site poses a significant challenge for small molecule inhibition.[23] Peptidomimetic analogues of the natural substrate are the most potent inhibitors developed so far.[24] These covalently inactivate the $3C^{pro}$ through the binding of a Michael acceptor to the catalytic cysteine. Yet, their inherent poor pharmacokinetic properties due to their peptidic nature limit the clinical utility and render the development of non-peptidic inhibitors a key objective.[25]

Results & Discussion

Covalent pharmacophore model and fragment screening

In order to enable the 3D pharmacophore-based identification of covalent fragments, a novel chemical feature type was introduced to our pharmacophore modeling software LigandScout.[26] First, covalently binding substructures were assembled from literature.[27-29] Despite the huge number of reported covalently binding ligands and substructures, the reaction mechanisms of the majority can be assigned to one of the following categories: (i) Michael addition, (ii) acylation, (iii) acetal/ ketal formation, (iv) alkylation, (v) boronic ester formation, (vi) sulfonylation. Thereby, covalently binding substructures, which are not applicable for rational design were discarded. This includes (i) overly reactive moieties, which are prone for unspecific binding such

as alkyl halides, (ii) covalent interactions that depend on prior transformation through the enzyme, (iii) substructures, which undergo complex transformations and (iv) high reactivity variability due to leaving groups. For the selected warheads, SMARTS patterns were developed and implemented in LigandScout. The covalent bond feature is represented by an orange sphere, which is placed on the ligand atom covalently bound or binding to the protein (figure 1A).

From crystal structures of peptidic ligands covalently bound to the CVB3 $3C^{pro}$ (see experimental section), a 3D pharmacophore model was generated, which comprises the essential non-covalent interactions and in addition reflects the necessary spatial positioning of the warhead moiety for covalent interaction with the catalytic Cys147 of the $3C^{pro}$. The model was subsequently statistically validated by using non-peptidic ligands reported in the literature and has a high specificity of 0.87 and sensitivity of 0.99 (see supporting information).[30-32] This shows that the model, which was derived from co-crystallized peptidic ligands, is able to retrieve bioactive, non-peptidic $3C^{pro}$ inhibitors (figure 1C). The interactions comprised in the final model are (i) covalent bond with the catalytic Cys147, (ii) hydrogen bonds to His161 and Thr142, which mimic the interaction of the P1-glutamine in the S1 pocket and (iii) lipophilic contacts in the S2 pocket (figure 1B).

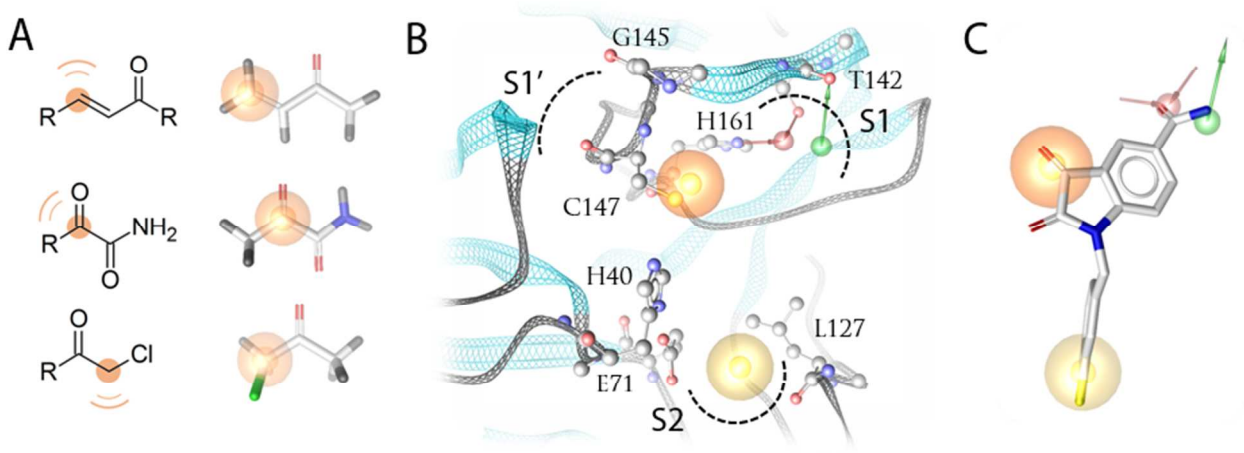

Figure 1. **Covalent 3D pharmacophore model captures 3C^{pro} binding characteristics.** (A) Common covalently binding substructures matched by the novel covalent bond feature type implemented in LigandScout, depicted in 2D and 3D. From top to bottom: Michael acceptor, α-ketoamide, α-halomethyl ketone, (B) Validated 3D Pharmacophore model for covalent 3C^{pro} binding. Orange sphere indicates covalent interaction, yellow spheres lipophilic contacts, red arrows hydrogen bond acceptors and green arrows hydrogen bond donors, respectively. (C) Active set molecule aligned to 3C^{pro} 3D pharmacophore model.

The generated 3D pharmacophore model was subsequently used to screen an in-house small molecule collection, which was pruned prior to the virtual screening to ensure fragment-like characteristics (relaxed rule of 3) and to remove PAINS-containing compounds. [33] [34] This resulted in approximately 3000 fragment-like molecules, which were included in the 3D pharmacophore-based virtual screening. Forty seven virtual hits were retrieved, which were further analyzed through covalent and non-covalent docking into the 3C^{pro} active site. For 19 fragments binding conformations of the initial and the covalent complex were retrieved, in which the interaction of the 3D pharmacophore model are formed. These 19 fragments represent 12 different chemotypes. From each of these, one fragment was selected for biological evaluation in an enzyme kinetic assay for 3C^{pro} inhibition (supporting information, figure S1A). Six fragments

inhibited the $3C^{pro}$ by more than 30 % at 650 µM (supporting information, figure S1B). One fragment (**F1**) showed a concentration- and time-dependent activity with an apparent IC_{50}* of 355 ± 30 μM. The time dependency is indicated by the flattening of the progress curve, which is a key characteristic of covalent binding (figure 2C). The covalent interaction results from the ketone moiety of **F1**, which can form a reversible thiohemiketal with Cys147 of $3C^{pro}$ (figure 2A). This is facilitated through the occupation of the S1 pocket by the primary amide moiety of **F1** forming the crucial hydrogen bonds to His161 and Thr142. Further investigations of the time-dependency of the $3C^{pro}$ inhibition by **F1** were performed through incubation experiments: The enzyme was incubated with the fragment for different time periods prior to starting the enzymatic reaction. For **F1**, each longer incubation periods resulted in a greater reduction of $3C^{pro}$ activity in the subsequent enzymatic assay. However, during the progress of the enzymatic reaction, $3C^{pro}$ activity increased for samples with longer incubation periods (figure 2D).

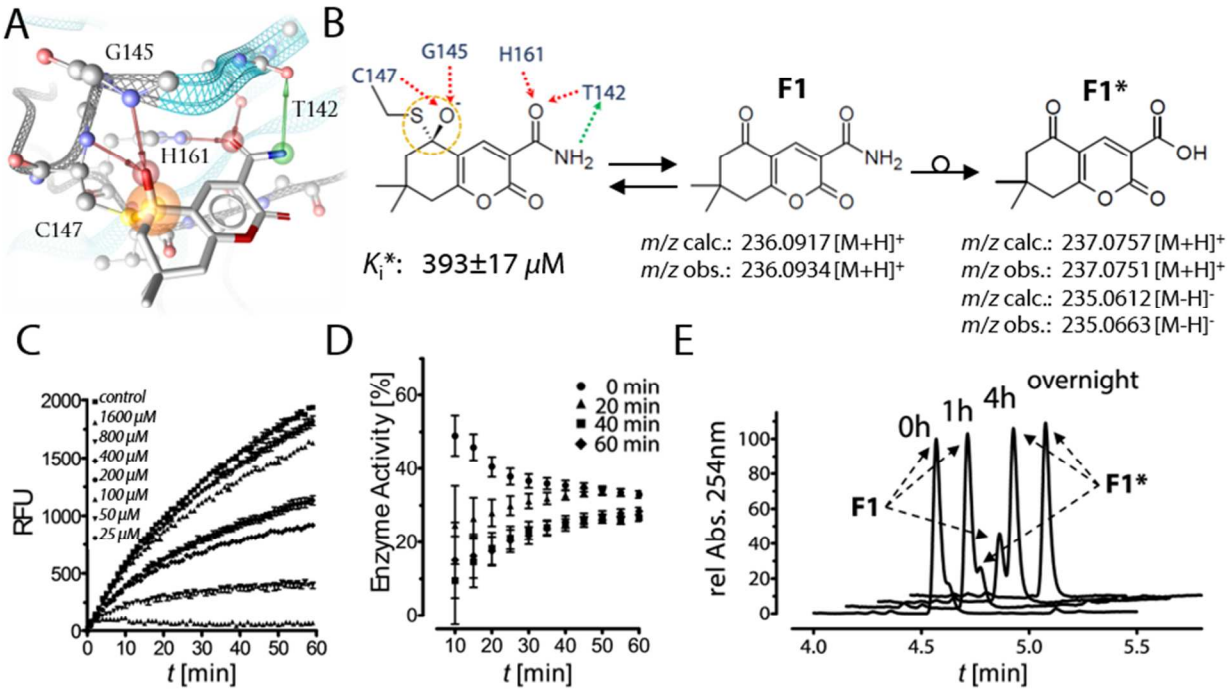

Figure 2. **Fragment hit F1 shows time-dependent 3C^{pro} inhibition through formation of a thiohemiketal.** (A) Proposed covalent binding conformation of **F1** in the active site of 3C^{pro} with interactions depicted as 3D pharmacophore features. (B) 2D depiction of the interactions in the reversible covalent complex of **F1.** Theoretical and experimentally observed *m*/*z* values for **F1** and instability reaction product **F1*** depicted with its putative structure. (C) Progress curves for the enzyme reaction in the presence of different concentrations of **F1**. (D) Relative enzymatic activity of 3C^{pro} in the progress of the enzymatic reaction after incubation with **F1** at 500 μM for 60 min (diamond), 40 min (square), 20 min (triangle) or 0 min (circle). (E) Superimposed HPLC chromatograms of **F1** after incubation in assay buffer for 0 h, 1 h, 4 h and overnight. Peaks for **F1** and the instability reaction product **F1*** are indicated.

The time-dependent behavior of **F1** was further investigated through stability analysis using LC/MS. Results indicate that overnight incubation of **F1** in aqueous assay buffer resulted in degradation into its carboxylic acid derivative **F1*** (figure 2B, E). High resolution MS show a difference in the *m*/*z* values of ~1 Da between **F1** and **F1*** as well as an increased ion count in

the negative mode. This structure fits the detected *m/z* values in the positive and negative mode, respectively. Since deamidation reactions do not occur easily, we surmise the reaction to occur via a hydrolytic opening of the labile lactone moiety and recyclization under deamination (supporting information, figure S2). This mechanism is in accordance with a reported synthesis scheme for chromene-3-carboxamides such as **F1**.[35] Furthermore, the conversion of the amide to an acid would explain the observed reduction in activity after incubation and thus confirm the proposed binding conformation. SAR data for S1 pocket binding suggests a 50-fold reduction in activity for the exchange of the primary amide group to an acid.[31, 36] In addition, the observed time-dependent activity of **F1**, the initial increase as well as the decrease alongside its decay, are in accordance to the proposed formation of a reversible covalent thiohemiketal. However, this prevents further confirmation of the covalent binding through mass spectrometry and the chemical instability of **F1** limits the attractiveness of this scaffold for further investigations.

Scaffold hopping

In order to identify bio-isosteric fragments to **F1**, a search for analogues was performed through substructure-based scaffold hopping.[37] The essential $3C^{pro}$ binding features of **F1**, the covalently binding ketone moiety and the primary amide group for S1 pocket hydrogen bonds, were transferred into a SMARTS pattern and used to filter commercial fragment collections (figure 3A). This led to the identification of a five-membered heterocycle-based scaffold. The essential primary amide and ketone moieties are arranged in a meta-substitution pattern, which enables the respective fragments to match the 3D pharmacophore model and to adopt the binding conformation of **F1** in the $3C^{pro}$ active site. From the initially identified fragments of this scaffold, five were commercially available from a single vendor and thus purchased for biological evaluation (figure 3B). Single concentration measurements revealed an apparent

activity cliff.[38] Fragment **C5** almost completely inactivates the $3C^{pro}$ at 650 µM, whereas none of the other fragments showed more than 20 % inhibition. Dose-response measurements for **C5** showed reasonable concentration-dependent activity with an apparent IC_{50} in the low three-digit micromolar range (figure 3D) and incubation experiments confirmed the time-dependent mode of action (figure 3E). Plots of the observed inactivation rate against the concentration of **C5** proceed through the origin indicating an irreversible interaction with the $3C^{pro}$ (figure 3F). This result provides an explanation for the apparent difference in biological activity within the set of fragments. However, it also causes suspicion for binding specificity as **C5** does not contain an apparent irreversible warhead and is highly similar to the other analyzed fragments, especially **C4** and **C6**.

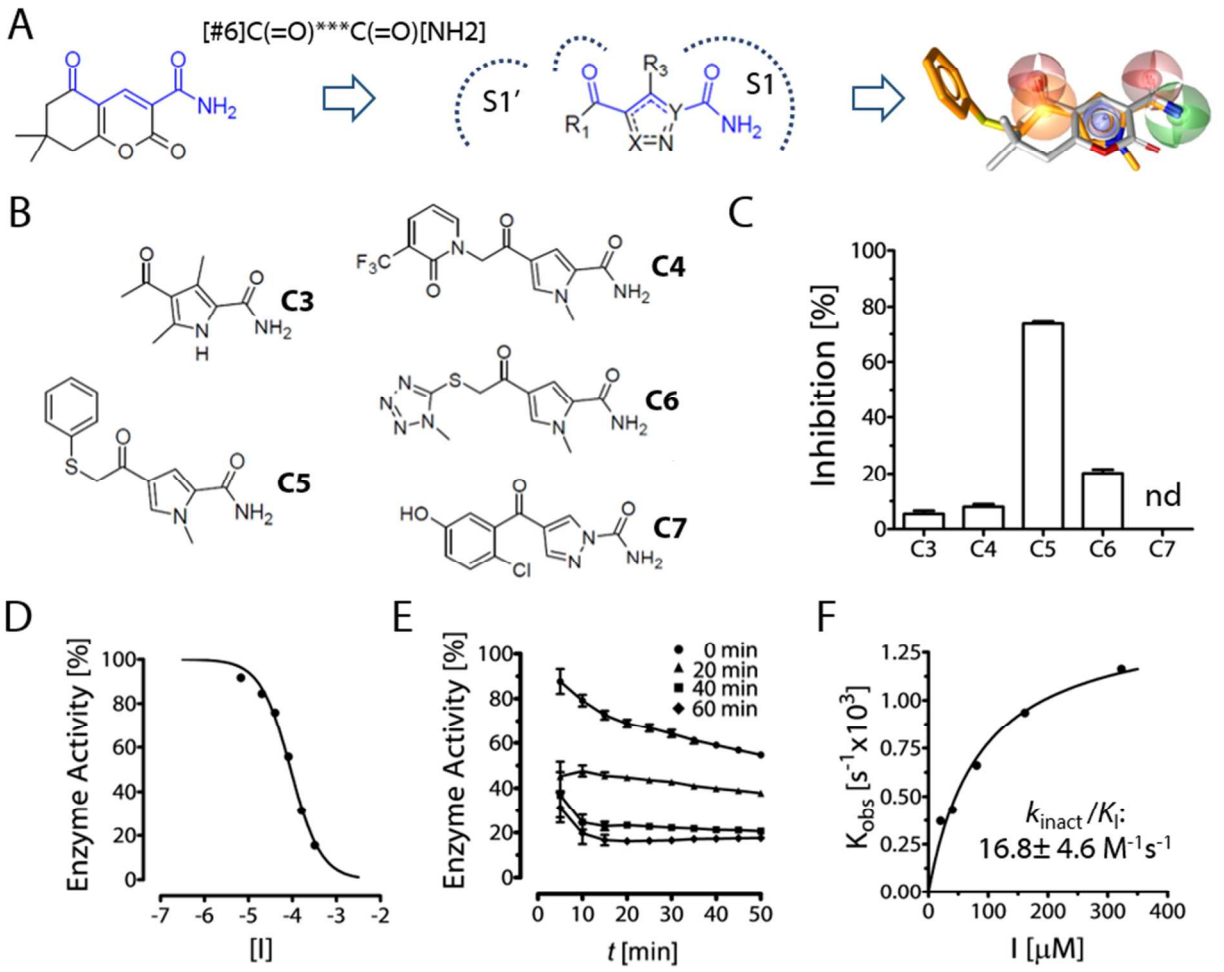

Figure 3. **F1 analogue search through scaffold hopping enabled identification of irreversible 3C^{pro} inhibitor C5.** (A) SMARTS substructure pattern utilized for scaffold hopping matched for **F1** and five-membered heterocycle. Matched substructure is colored in blue. 3D pharmacophore-based superimposition of **F1** and a pyrrole-based fragment. (B) Selected fragments and (C) relative 3C^{pro} inhibition at 650 μM. Inhibition for **C7** was not determined (nd) due to solubility issues. (D) Dose-response curve for **C5**. (E) Relative enzymatic activity of the 3C^{pro} in the progress of the enzymatic reaction after incubation with **C5** at 100 μM for 60 min (diamonds), 40 min (square), 20 min (triangle) or 0 min (circle). (F) Plot of k_{obs} against the concentration of **C5** and inactivation rate (k_{inact}/K_I) calculated from the slope of the linear part of the curve.

Protein mass spectrometry was performed to investigate the binding of **C5**. Deconvolution of the obtained mass spectra revealed three components (figure 4A): One with the mass of the apo $3C^{pro}$ (21456 Da) and two components with greater masses, 21620 Da and 21562 Da, respectively. The increase in mass equals the molecular weight of **C5** for none of the compounds, which nourished suspicion concerning the specificity of inhibition. However, we were able to propose a putative mode of action through detailed analysis of the structural differences of the fragments and the increase in mass for the different adducts detected. The major difference of **C5** to the other fragments is the α-methyl ketone substituent, which is a thiophenol group in **C5**. Its molecular weight of 109 Da equals the increase in mass for the minor adduct. Furthermore, the mass shift for the major mass peak is 165 Da, which equals the fragment **C5** mass (275 Da) except the 109 Da of the thiophenol moiety. Based on this observation, we reasoned that **C5** reacts similarly to other activated methyl ketones (figure 4B). The attack of the cysteine thiolate leads to the formation of an irreversible thioether at the α-carbon of the ketone moiety of **C5** through displacement of the thiophenolate. This irreversible reaction product shows the same mass shift as the major peak (+165 Da). In addition, the displaced thiophenolate can react with the cysteine through the formation of a disulfide, which equals the mass shift detected for the minor product (+109 Da). High resolution MALDI/TOF mass spectrometry further confirmed the exact masses and mass shifts for the $3C^{pro}$-**C5** reaction adducts (figure 4C).

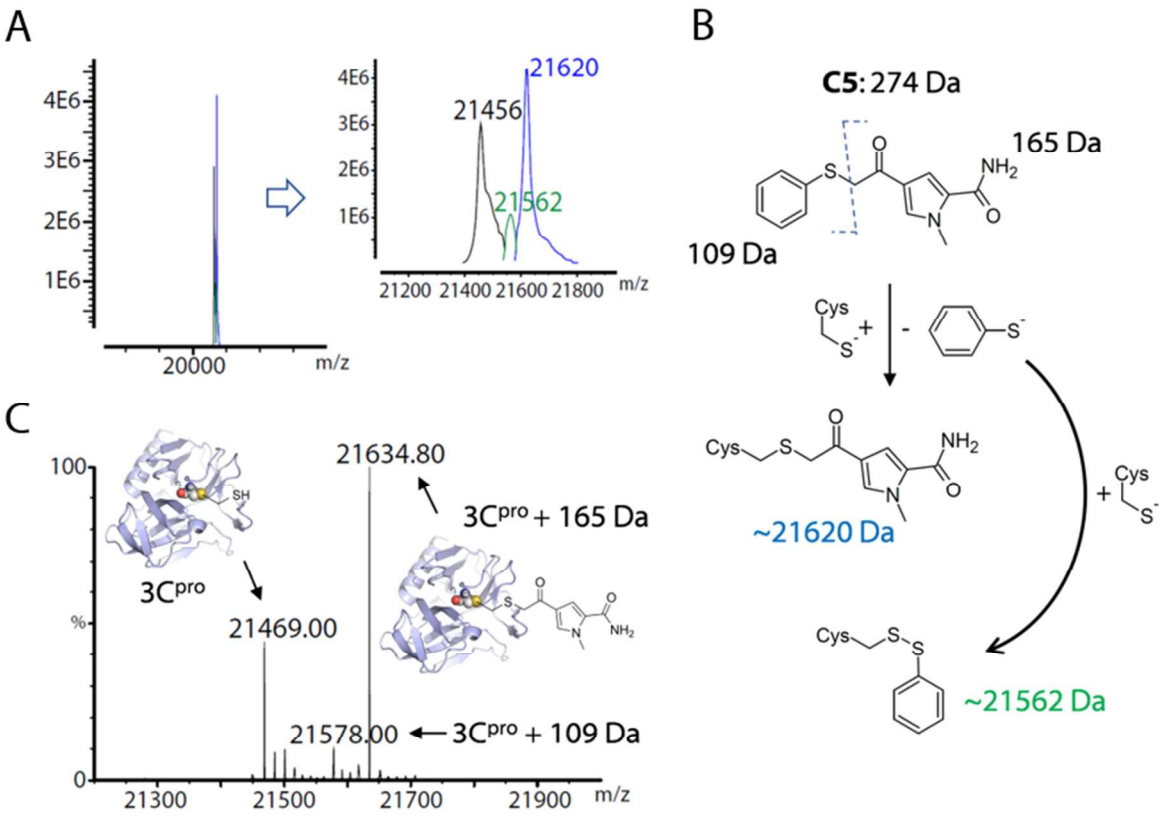

Figure 4. **Mass spectrometry reveals irreversible 3C^{pro} binding by C5 through the displacement of thiophenol**. (A) ESI mass spectrum of the 3C^{pro} with **C5** after deconvolution. (B) Putative reaction mechanism for the formation of the 3C^{pro}-**C5** adducts. (C) Deconvoluted high-resolution MALDI-TOF spectra of the 3C^{pro} after incubation with **C5**. The main peak of 21634.8 Da corresponds to the thioether adduct formed after reaction of **C5** with the 3C^{pro}.

The MS data and the proposed reaction products provide a rationale for the determined biological activity of **C5** as an irreversible 3C^{pro} inhibitor as well as for the difference to the other selected fragments. To further rationalize the binding mode of **C5** the initially proposed binding hypothesis, based on the 3D pharmacophore model for covalent 3C^{pro} binding, was revisited. The initial hypothesis suggested the formation of a reversible thiohemiketal from a non-covalent complex in which the primary amide moiety forms the crucial hydrogen bonds to His161 and Thr142 in the S1 pocket and the ketone moiety is positioned in close proximity to the

catalytic Cys147 (figure 5A, B). In addition, the attack of the cysteine thiolate can also occur at the α-carbon of the ketone moiety of **C5** in the initial non-covalent complex. This leads to the irreversible thioether product detected in the mass spectrometry through a S_N2 reaction via the displacement of thiophenolate. Covalent docking shows that the amide moiety of thioether product is able to form the crucial hydrogen bonds in the S1 pocket and thus indicates a conserved binding mode confirming the 3D pharmacophore-based binding hypothesis (figure 5C).

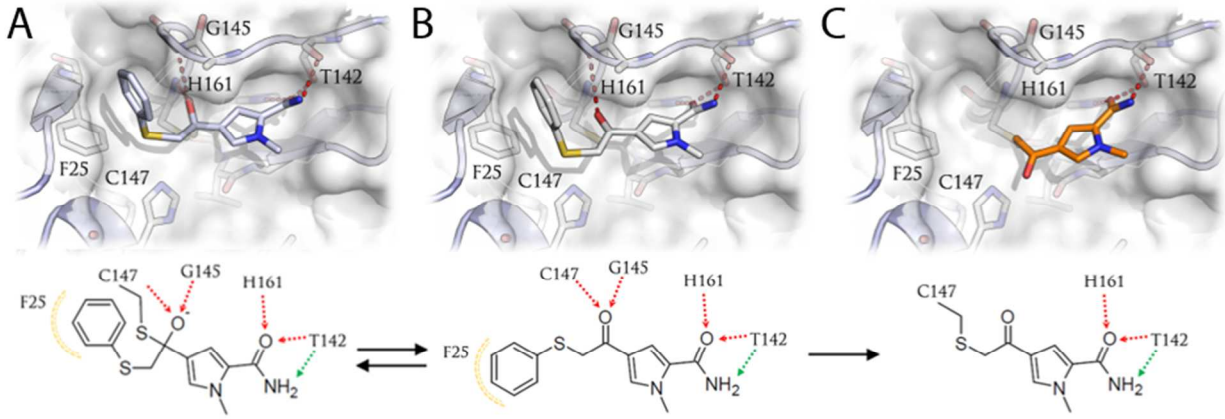

Figure 5. **Proposed covalent binding mode of C5**. 3D (top) and 2D (bottom) depictions of the complexes and interactions formed between C5 and the 3Cpro. Interactions are described as pharmacophore features. Yellow spheres indicate lipophilic contacts, orange sphere indicates covalent bond formation, green and red arrows indicate hydrogen bond donor or acceptor functionalities.

The biological activity and the observed activity cliff result from the formation of an irreversible thioether by **C5** through its α-phenylthiomethyl ketone moiety, which, to our knowledge, has not been reported to date.

Fragment optimization & warhead analysis

To further investigate the binding mechanism of **C5** and to increase $3C^{pro}$ inhibition potency, synthetic fragment optimization was performed. Based on the proposed binding model, growing vectors for **C5** were defined to occupy additional pockets in the $3C^{pro}$ active site, which include the adjacent S2 and S4 pocket, respectively (figure 6A). The pyrrole nitrogen of **C5** represents a putative synthetic handle for the incorporation of additional functionalities to occupy the aforementioned pockets as the methyl substituent does not contribute to $3C^{pro}$ binding and thus can be substituted. A *de novo* design workflow was developed for the rational design of pyrrole substituted **C5** analogues occupying the adjacent pockets while maintaining the original binding mode. Hereby, synthesis-tailored transformation rules, encoded as SMIRKS patterns, are applied in combination with tangible building blocks to generate virtual libraries of synthetically feasible compounds. For the design of **C5** analogues, its nor-derivative was used as starting point for the *de novo* design workflow, in which it was transformed via nucleophilic substitution at the pyrrole nitrogen with alkyl halide building blocks (figure 6B). The obtained virtual library of approximately 2000 N-alkylated **C5** analogues was virtually screened using the initial 3D pharmacophore model, which comprises the essential hydrophobic contacts to Leu127 for S2 pocket binding through a lipophilic feature (figure 1B). 3D pharmacophore matching hits were subsequently docked in all three putative binding states to confirm formation of the crucial hydrogen bonds in the S1 pocket (figure 6C). The final selection of **C5** analogues occupy the S2 pocket through lipophilic pyrrole substituents, which range from a flexible phenyl alkyl ether to rigid biphenyl methyl moieties. The corresponding commercially available alkyl halide building blocks are depicted in figure 6D.

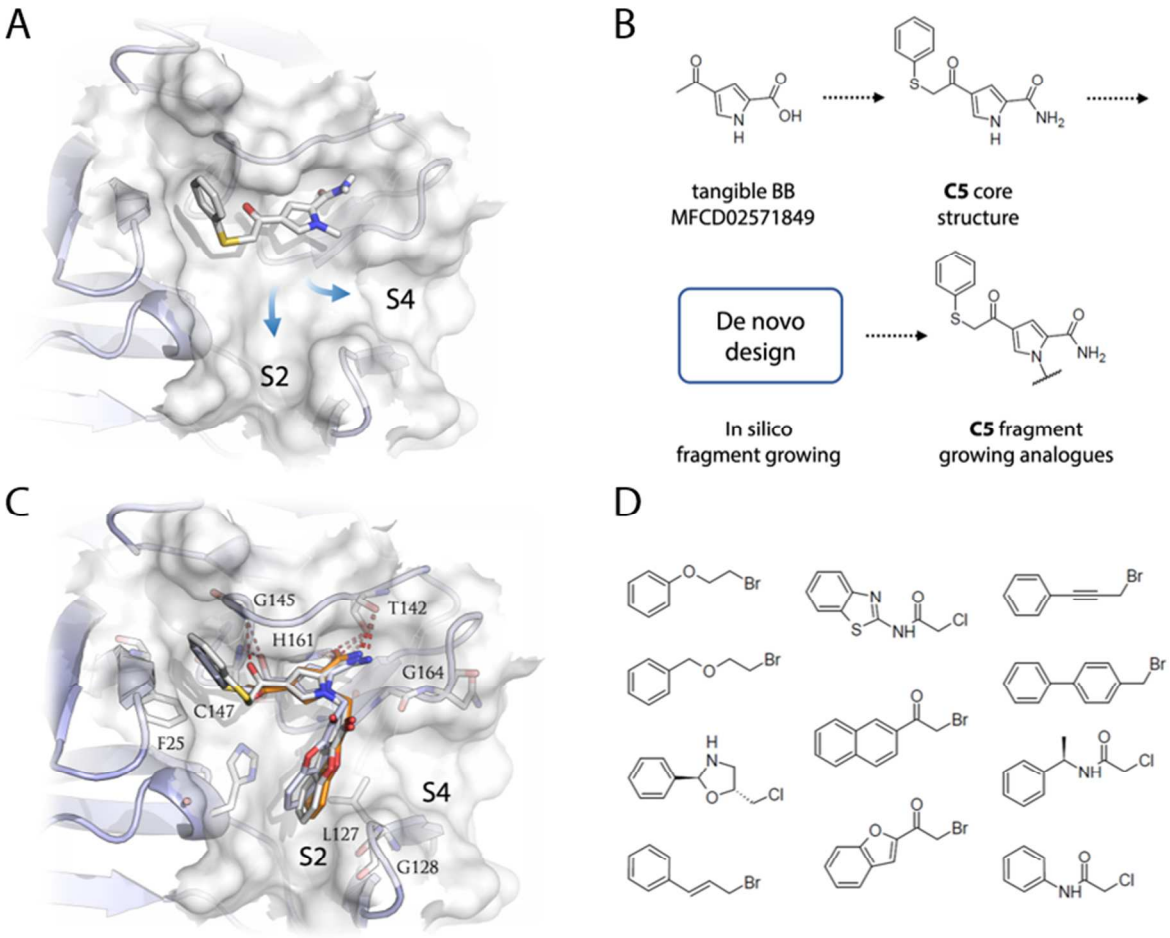

Figure 6. **C5 fragment growing in 3C^{pro} active site driven by de novo design.** (A) Non-covalent binding conformation of **C5** and growing vectors toward S2 and S4 pocket, respectively. (B) **C5** fragment growing scheme starting from putative chemical synthesis precursor, input structure for *de novo* design-based fragment growing and generalized structure of virtual **C5** analogues with variable pyrrole substituent. (C) Docking poses of a representative fragment growing analogue of **C5** occupying the S2 pocket of the 3C^{pro}. All three binding states are shown: Initial complex (white stick coloring), thiohemiketal intermediate (light blue stick coloring) and final thioether (orange coloring). Hydrogen bonds are indicated by red dashed lines. (D) Chemical structures of commercially available building blocks utilized in the *de novo* design of virtual screening hits for the S2 pocket.

The synthesis of the *de novo* designed **C5** analogues addressing the S2 pocket was conducted according to scheme 1. From the commercially available methyl 2-pyrrole-carboxylate **1** the ketone **2** was generated through Friedel-Crafts acylation. N-Alkylation with the respective alkyl halide led to the N-substituted ester **3**, which was converted into the corresponding primary amide **5** via the free acid **4**. The phenylthiomethyl ketone **7** was obtained from the reaction of the bromomethyl ketone **6** with thiophenol under basic conditions. For the synthesis the alkyl bromides and among those the benzylic and bromomethyl ketones were prioritized due their higher reactivity for the pyrrole N-alkylation. The second ketone moiety proved to challenging for the selective bromination step. By using 1-bromo-3-phenyl-propene, a first **C5** analogue **7a** was synthesized. In addition, the double substituted 2,2-bis-(phenylthiol) methyl ketone **8a** was also obtained using an excess of thiophenol. This unintentionally synthesized analogue provided the opportunity to assess the specificity of the phenylthiomethyl ketone warhead, which was extended by including the synthesis intermediates **5a** and **6a**.

Scheme 1: Scheme for the synthesis of the **C5** analogues.

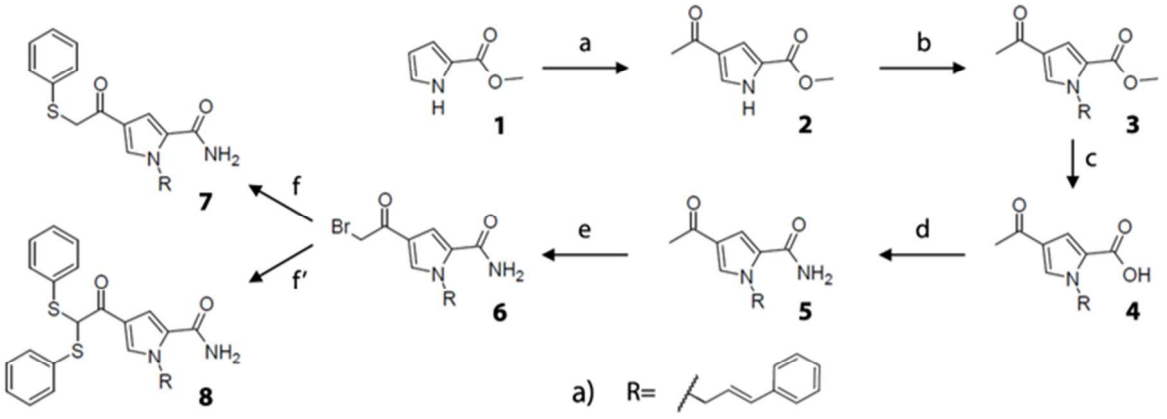

Reagents and conditions: (a) $AlCl_3$, CH_3COCl, DCE, rt; (b) K_2CO_3, alkylhalide, DMF; (c) KOH, MeOH, THF; (d) $(COCl)_2$, NH_3, THF; (e) PTTB, THF; (f) K_2CO_3, DMF, C_6H_5SH.

The biological evaluation showed activity against the CVB3 $3C^{pro}$ for all four synthesized compounds with a time-dependent mode of action. **5a** and **8a** showed reversible $3C^{pro}$ inhibition

with K_i values of 197±8 μM and 272±8 μM, respectively. In contrast, **6a** and **7a** were irreversible $3C^{pro}$ inhibitors with k_{inact}/K_I values of 1,707±33 $M^{-1}s^{-1}$ and 54.4±3.8 $M^{-1}s^{-1}$, respectively (Table 1). The irreversible binding of the phenylthiomethyl ketone **7a** provides an initial confirmation of the proposed binding mechanism of **C5**. In contrast, the 2,2-bis-(phenylthiol) methyl ketone **8a** is a reversible $3C^{pro}$ inhibitor, in an analog way to per-halomethyl ketones. These are reversible inhibitors in contrast to their mono-halogenated analogues, such as the bromomethyl ketone **6a**, which binds irreversibly.[28] Furthermore, the bulkiness of the thiophenol substituents of **8a** potentially hampers the covalent binding as **8a** is only as active as the significantly smaller ketone **5a**. This is less active than the fragment hit **C5**, which is due to the missing thiophenol leaving group. Thus, the effect of the introduction of the phenylpropenyl substituent is only possible by comparison to the other pyrrole-based fragments devoid of a leaving group. These were inactive at 650 μM showing a significant boost in activity through occupation of the S2 pocket by **5a**. However, the increase of the k_{inact}/K_I value from **C5** to **7a** is only threefold, which raises questions about the contribution of the phenylpropene substituent for **7a**.

Table 1. C5 and synthetic analogue $3C^{pro}$ inhibition values and binding kinetics (nd: not determined).

ID	K_i [μM]		k_{inact}/K_I [$M^{-1}s^{-1}$]		Binding kinetics
	CVB3	EV D68	CVB3	EV D68	
C5	-	-	16.8 ± 5	21.3 ± 8	Irreversible
5a	197 ± 8	422 ± 8	-	-	Reversible
6a	-	-	1,707 ± 33	1,214 ± 12	Irreversible
7a	-	-	54.4 ± 4	160 ± 26	Irreversible
8a	272 ± 8	nd	-	-	Reversible

The activity of the synthesized analogues was additionally investigated using a second 3C protease from the enterovirus D68 (EV D68). This $3C^{pro}$ has an overall sequence similarity of 67 % and all residues relevant for ligand binding in the active site are conserved so that a highly similar binding mode can be assumed (Supporting information, figure S4). The crucial distinction to the CVB3 $3C^{pro}$ is the presence of a non-catalytic cysteine residue (Cys60) allowing for additional exploration of the reaction specificity of the irreversible inhibitors. Evaluation of the EV D68 $3C^{pro}$ inhibition revealed comparable inhibition values (Table 1). The phenylthiomethyl ketones **C5** and **7a** show slightly increased k_{inact}/K_I values of 21.3±8 $M^{-1}s^{-1}$ and 160.4±26 $M^{-1}s^{-1}$, respectively. In contrast, the k_{inact}/K_I of **6a** is reduced by one third to 1,214±12 $M^{-1}s^{-1}$ and it shows a steep curvature of the dose-response plot with a Hill slope of 1.8 indicating unspecific or multiple binding events (Supporting information, figure S5A). Mass spectrometry was performed for EV D68 $3C^{pro}$ after incubation with the irreversible inhibitors to investigate this hypothesis further (figure 7). For the apo EV D68 $3C^{pro}$ a single peak of 21261.26 Da was found. After reaction with **6a**, two main peaks occur at 21527.6 Da and 21793.67 Da, respectively. These correspond to mass shifts of 266 Da and 532 Da, respectively, which is twice as much as the former. The mass shift of 266 Da equals the mass of **6a** except for the bromine. Thus, the peaks reflect single and double binding of **6a** through unspecific reaction with either cysteine residue. In contrast, for **7a** only one peak with 21527.05 Da was found in addition to the apo mass peak. The mass shift of 266 Da corresponds to the mass of **7a** except the thiophenol moiety and thus a single reaction of **7a**. This putatively exclusively occurs via the catalytic Cys147 as this is more reactive than Cys60 and secondly due to the binding kinetics of **6a** with the high Hill slope indicating that Cys60 binding does not affect the $3C^{pro}$ activity. Only a single adduct peak of 21426.13 Da was detected for **C5** with a mass shift of 164 Da, the same as

determined for the CVB3 $3C^{pro}$, which confirms the proposed binding mechanism and reaction specificity of the phenylthiomethyl ketone warhead for catalytic cysteine residues.

The k_{inact}/K_I value increase from **C5** to **7a** is greater for the EV D68, yet the small abundance in the mass spectrum of **7a** indicates a smaller rate of irreversible binding in comparison to **C5**. Thus, the increase in activity can be attributed to better non-covalent interactions due to the phenylpropene substituent and a better K_I.

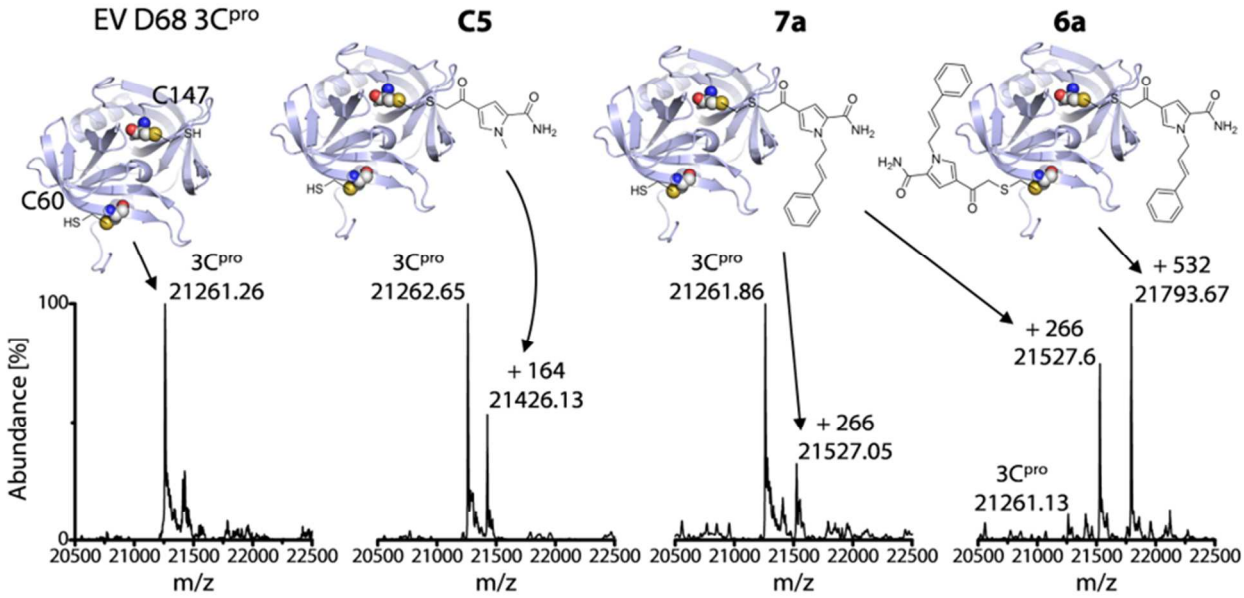

Figure 7. **EV D68 $3C^{pro}$ binding of C5 and synthesized analogues elucidated by mass spectrometry.** Deconvoluted ESI/QTOF mass spectra of EV D68 $3C^{pro}$ apo structure and after incubation with **C5**, **7a** and **6a** (from left to right). Main peaks are labeled with corresponding *m*/*z* value. Schematic depictions of EV D68 $3C^{pro}$ or $3C^{pro}$-inhibitor adducts are shown to indicate binding to catalytic Cys147 or non-catalytic Cys60, respectively. Note that the single adduct peak of the **6a** MS results from binding to either cysteine residue.

The reaction specificity of the phenylthiomethyl ketone moiety was further investigated through its reaction with the nucleophile glutathione (GSH) (figure 8B). This biologically

ubiquitous tripeptide contains a cysteine thiol moiety and can thus react in analogy to the cysteines of the 3C proteases. In addition to the active ligands **C5** and **7a**, available phenylthiomethyl ketone bearing fragments were included in the analysis (Figure 8A). **C8** was taken from our in-house small molecule collection and **C9** was prepared through a single-step synthesis from 2-bromoacetophenone and thiophenol. Both compounds do not show activity against the CVB3 $3C^{pro}$ in the micromolar range (Supporting information, figure S5A). Furthermore, the synthesized 2,2-bis-(phenylthiol) methyl ketone **8a** and the bromomethyl ketone **6a** were analyzed. Each compound was incubated with GSH (2.5 mM) at an equimolar concentration. The reaction was monitored via LC/MS for 24 h (Figure 8C). The formation of new entities or a reduction of the initial compound could only be detected for **6a** within the analyzed time period (figure 8E). For **6a**, a second peak with a smaller retention time appears, whereas the peak of the original compound vanished. This indicates the formation of reaction product between **6a** and GSH. This is supported by the *m*/*z* of the ions in the MS spectra of the new peak, which fit the calculated *m*/*z* of a reaction product formed through the nucleophilic attack of the thiol moiety at the bromomethyl ketone group and displacement of the bromine (figure 8D). This reactivity of **6a** is known and was used for the synthesis of the desired compound **7a**. It also served as positive control for this analysis as the same GSH-adduct with the same *m*/*z* and retention time would have been formed by **7a**.

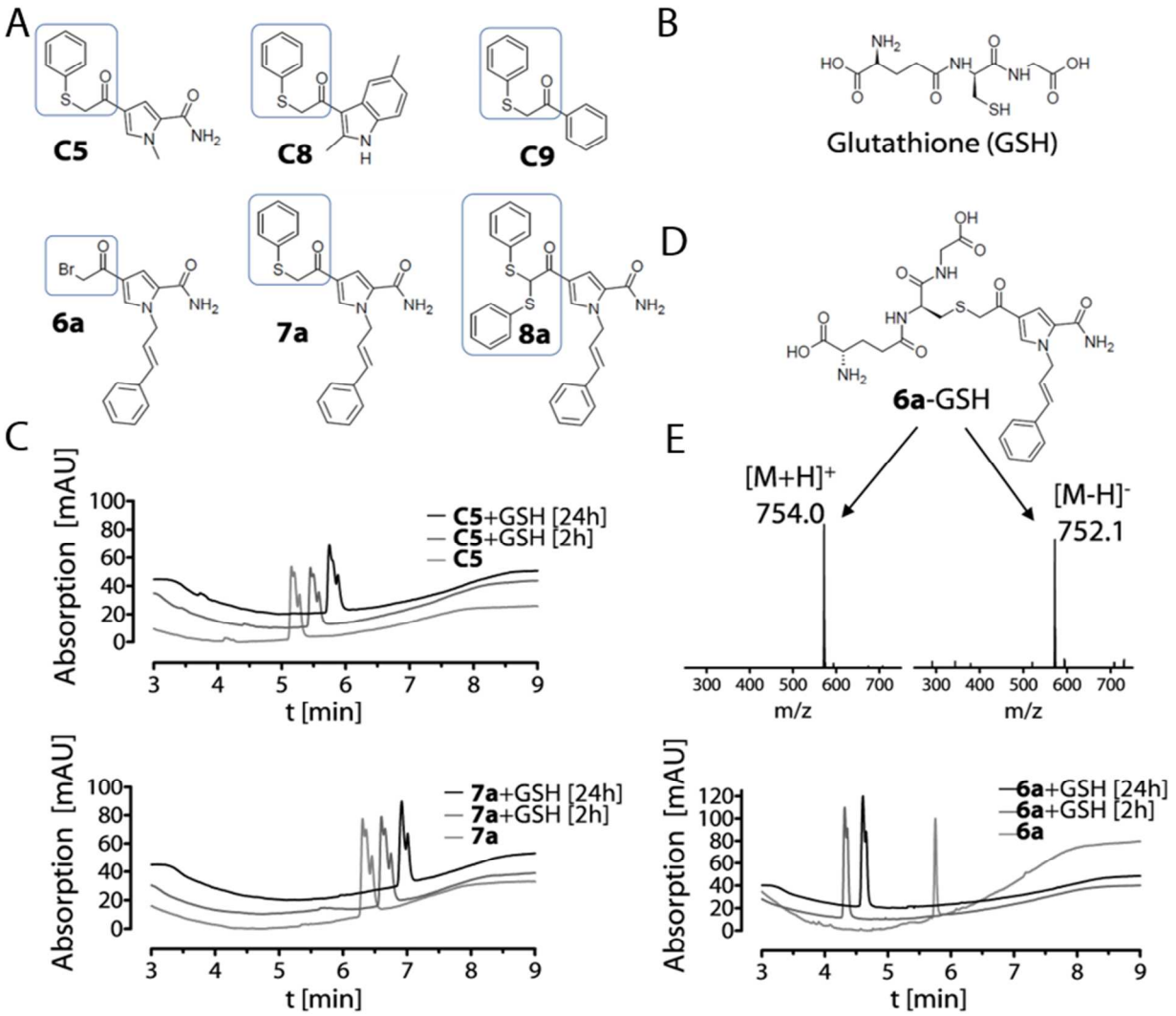

Figure 8. **Phenylthiomethyl ketones are stable in glutathione assay checking warhead reaction specificity.** (A) Assembled set of activated α-substituted methyl ketones, warhead substructure is highlighted by blue frame. (B) Chemical structure of the nucleophile glutathione (GSH). (C) Superimposed LC chromatograms of **C5** (top) and **7a** (bottom) without (gray) and after incubation with GSH for 2 h (dark gray) and 24 h (black). (D) Chemical structure of the putative reaction product **6a**-GSH. (E) Mass spectra of the reaction product **6a-GSH** in the positive (right) and negative mode (left) with relevant ions and *m*/*z*. Superimposed LC chromatograms of **6a** without (gray) and after incubation with GSH for 2 h (dark gray) and 24 h (black).

Binding mechanism

The reaction of the phenylthiomethyl ketones with the $3C^{pro}$ can lead either to the formation of a reversible thiohemiketal or an irreversible thioether through S_N2 displacement of the thiophenol moiety. The differences in the biological activity and irreversible binding between **C5** and **7a** can be explained by a higher affinity of **7a** in the thiohemiketal state and slower displacement of the thiophenol moiety in comparison to **C5**. The introduction of the phenylpropenyl substituent in **7a** apparently stabilizes the thiohemiketal and thus reduces the formation of the irreversible thioether product detected by mass spectrometry. This preference of **7a** for the thiohemiketal is supported by docking studies, which show that the positioning of the phenylpropenyl moiety may vary for the covalent binding products (figure 9A-C). This is due to the difference of the ligand atom covalently bound to the catalytic cysteine. The necessary formation of the hydrogen bonds in the S1 pocket requires a slight perturbation of the phenylpropenyl substituent occupying the S2 pocket in the thioether product (figure 9C). This does not apply for the binding of **C5** due to the insignificant contribution of its N-methyl substituent. Therefore, the formation of the thioether through displacement of the thiophenol moiety is slower for **7a**, which reduces the benefit of the warhead in comparison to **C5**.

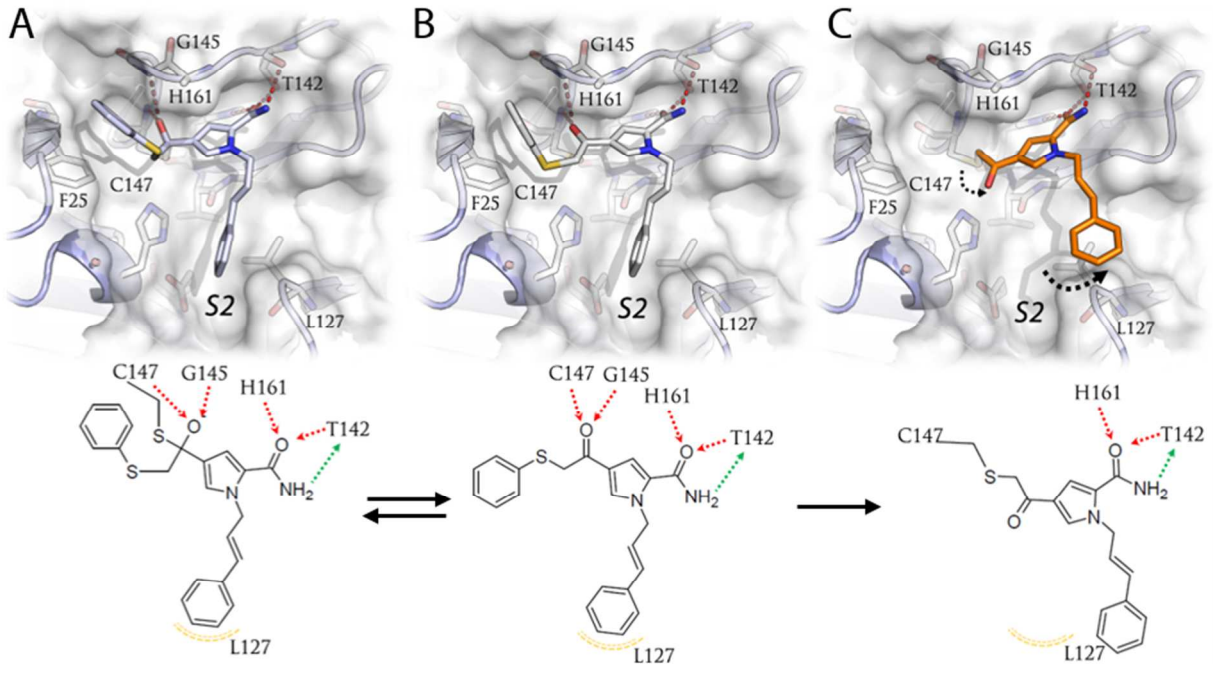

Figure 9: **Perturbation of S2 occupation for the different covalent products of 7a.** 3D (top) and 2D (bottom) depiction of the three complexes formed during the $3C^{pro}$ binding by **7a**. Dashed arrow indicates the repositioning of the phenylpropenyl substituent during the formation of the thioether. Hydrogen bonds are indicated as red dashed lines in the 3D depiction. Yellow lines indicate lipophilic contacts.

The glutathione reaction analysis as well as the mass spectrometry data show specificity of the phenylthiomethyl ketone reactivity for catalytic cysteines. This implies that the covalent binding results from the proper spatial positioning of the warhead in the initial complex of the bioactive thiophenolmethyl ketones **C5** and **7a** comprising the essential chemical features, especially the primary amide moiety for S1 pocket binding. In addition, the thiophenol moiety seems to be favorable for occupying the S1' pocket as the pyrrole-based fragments **C4** and **C6**, which only differ in the α-substituent, are virtually inactive. Especially since the S_N2 displacement reaction would rather suggest the N-methyltetrazolethiol substituent of **C6** to be a better leaving group

due to its higher acidity in comparison to the thiophenol moiety. However, the influence of the catalytic mechanism for the unusual reaction and specificity of the phenylthiomethyl ketone with the $3C^{pro}$ is not clear especially as it has also been reported to be an unreactive warhead for other targets.[39] This would require further analyses to assess its impact for the displacement of the thiophenol and to verify the proposed binding mechanism. The evaluation of a broader range of leaving groups such as the related dimethylsulfonium methyl ketones would be insightful to explore the factors of the irreversible 3C protease inactivation by activated methyl ketones.

Conclusion

The presented study reports the identification of covalently binding fragments for enterovirus 3C protease through the use of 3D pharmacophores with novel chemical features representing potential covalent linkage. The combination of features for covalent and non-covalent interactions reflects the general consideration for the relevance of the initial, non-covalent complex in the design of specific, K_I-driven covalent inhibitors. Fragment hit validation and confirmation of the binding hypothesis through mass spectrometric analysis allowed for a rational, structure-based optimization in the absence of crystallographic data on the binding conformation. The synthesized analogue shows inactivation rates in the three-digit range against 3C proteases with a non-peptidic scaffold making it a promising starting point for further optimization.

Mass spectrometric analysis of selected fragments led to the identification of the phenylthiomethyl ketone moiety as a covalently binding substructure for irreversible 3C proteases inactivation. The binding kinetics of the discovered fragments and structural modelling suggest key relevance of the non-covalent interactions for the proper initial positioning of the phenylthiomethyl ketone warhead to enable the subsequent covalent binding through

displacement of the thiophenolate. This provides novel insights for the reaction of activated methyl ketones and extends the available range of leaving groups. The conducted experiments show considerable reaction specificity of the phenylthiomethyl ketone warhead, which suggests an application for the selective covalent inactivation of target proteins or for activity-based protein profiling.

Experimental procedures

Reagent sources and quality assessment: Commercially available fragments were purchased from Enamine (Ukraine). The in-house small molecule collection was assembled by using a maximum common substructure concept based on bioactive molecules listed in the World Drug Index as reported by Lisurek *et al*.[40, 41] The compounds were purchased from ChemDiv Inc. (San Diego, USA). Purity >95 % and identity of the compounds was determined by LC/MS using an Agilent (Santa Clara, USA) 1100 LC/MS system equipped with a Luna-C18 RP-column (3 μm) by Phenomenex (Torrance, USA). Samples were prepared by mixing 1 μL of the inhibitor DMSO stock solution with 99 μL of a 1:1 mixture of water and acetonitrile. As solvents water and acetonitrile were used containing each 0.1 % (v/v) of formic acid. The ratio of water to acetonitrile was changed from 95:5 to 1:99 during the chromatographic run with a constant flowrate of 1 mL/min.

The small molecule collection was filtered by using a KNIME workflow with the following physicochemical property cut offs, calculated by RDKit KNIME nodes: Molecular weight ≤325 Da, heavy atom count ≤ 20 and cLogP ≤ 3.[42, 43] Compounds were filtered for PAINS substructures by using in-house SMARTS patterns in a KNIME workflow based on reported substructures- and filters. [34 44]

3C^{pro} inhibition assay and evaluation: 3C^{pro} was expressed and purified as described previously.[15] The biochemical evaluation for CVB3 and EV D68 3C^{pro} inhibition was done by using the FRET substrate N-Dabcyl-KTLEALFQGPPVYE-(Edans)-NH_2 purchased from Biosyntan (Berlin, Germany). In 384 well plates (Corning, USA) 10 μL buffer consisting of 100 mM HEPES-NaOH, 1 mM EDTA and 0.01 % TritonX (v/v) at a pH of 7.5 were mixed with 10 μL of 3C^{pro} (40 μM), 10 μL of substrate, diluted in the assay buffer to a concentration of 20 μM, and either 1 μL of the inhibitor diluted in DMSO or only DMSO for the positive control. The fluorescence signal was measured at a wavelength of 538 nm after irradiation at 355 nm with a Safire II Fluorimeter (Tecan, Austria) over 30 min.

Each concentration was tested in triplicates and the obtained data was analyzed using GraphPad Prism. Apparent IC_{50} values were calculated by non-linear regression by using equation $v_i/v_0=1/(1+[I]/IC_{50})^h$, where v_i is the initial enzyme velocity, v_0 is the velocity in the absence of the inhibitor and [I] is the inhibitor concentration. Observed first-order rate constant k_{obs} values were calculated for covalent reversible inhibition by using equation $[P]=v_s t+((v_i-v_0)/k_{obs})(1-e^{(-k_{obs}t)})$, where [P] is the product concentration. K_i values were obtained from the ratio k_{off}/k_{on} according to equation $K_i= k_{off}/k_{on}$. k_{obs} values for irreversible inhibition were determined through equation $[P]=v_i/k_{obs}\ (1-e^{(-k_{obs}t)})$. The second order-rate constants k_{inact}/K_I were derived from the slopes of the linear part of the graph of k_{obs} as a function of the inhibitor concentration based on equation $k_{obs}/[I] = k_{inact}/K_I$, where k_{inact} is the rate of maximum enzyme inactivation at an infinite inhibitor concentration and K_I refers to the inhibitor concentration displaying half-maximum enzyme inactivation.

3C^{pro} incubation assay. For the incubation experiments the same reagents and quantities were used as described above. The protein solution was mixed with the inhibitor or DMSO for the

control in the assay buffer and covered with a lid to prevent evaporation. After 60, 40, 20 or zero minutes the enzymatic reaction was initiated by addition of the substrate and monitored for 60 min. The incubation was done in triplicated for each time frame of incubation and the respective control. The obtained data was analyzed using GraphPad Prism. The relative enzyme activity for every five-minute time step of the enzymatic reaction was calculated for every distinct time frame of incubation. The obtained relative enzyme activity was plotted as a function of the enzyme reaction time.

Glutathione reaction assay. At 2.5 mM the inhibitor, dissolved in DMSO, was mixed with an equimolar solution of glutathione dissolved in the assay buffer to a volume of 50 μL. The mixture was incubated at room temperature for 2 h and 24 h, respectively. After each incubation period an aliquot was analyzed via LC/MS as described above. Controls for each inhibitor were prepared and treated analogously, except the omission of glutathione.

Protein mass spectrometry. For protein mass spectrometry the same reagents were used as described above. For CVB3 $3C^{pro}$ MS 10 μL of the stock solution were mixed with 20 μL buffer and 1 μL of the inhibitor dissolved in DMSO, which was added at a concentration, leading to 50 % reduction of $3C^{pro}$ activity after 30 min in the kinetic assay. The samples were incubated for 60 min and then subjected to LC/MS analysis using the following procedure. For chromatographic separation, a Phenomenex Jupiter C-18 RP-column (5 μm) was used. As solvents water and acetonitrile were used containing each 0.1 % (v/v) of formic acid. The ratio of water to acetonitrile was changed from 95:5 within the first 35 min of the run to 1:99, which was kept constant for 5 min and then turn back to the initial ratio within the last 4 min of the chromatographic run. The flow rate was set to 0.5 mL/min. For ionization the following parameters were used: Capillary voltage 3.3 kV, sampling cone 40 V, source offset 60 V, source

temperature 100 °C, desolvation temperature 250 °C, desolvation gas flow 600 L/h. MaxEnt1 method of the MassLynx software (Waters Co., Milford, UK) was used for deconvolution of the obtained protein mass spectra.

For high resolution masses and the mass spectrometry of the EV D68 $3C^{pro}$ the following procedures were used. Small molecule samples were prepared as described above. For protein MS, 200 μL of EV D68 $3C^{pro}$ stock solution were mixed with 50 μL buffer and 10 μL of the inhibitor dissolved in DMSO, which was added at a concentration, leading to 50 % reduction of $3C^{pro}$ activity after 30 min in the kinetic assay. The samples were incubated for 60 min and subsequently concentrated and desalted through ultrafiltration using Roti®Spin MINI-10 devices from Carl Roth GmbH & Co. KG. For sample purification 1 mL of purified water was used. The sample was concentrated to a volume of 20-30 μL.

Sample measurements were performed using an Agilent HPLC/QTOF-MS instrument. The Infinity 1290 UHPLC equipped with a Phenomenex Jupiter C-18 RP-column (5 μm) was used for chromatographic separation. 10 μL of injected samples were eluted with a flow rate of 0.5 mL/min using a gradient of water and acetonitrile containing each 0.1 % (v/v) of formic acid, which was changed from 95:5 to 1:99 within 3 min of the chromatographic run. This was held constant for the next 6 min and then changed back within the next minute. The 6550 iFunnel QTOF was used for mass analysis with the following parameters of the electrospray ionization-source: Gas temperature 200 °C, gas flow 14 l/min, nebulizer gas at 35 psig, sheath gas temperature 350 °C, sheath gas flow 11 L/min, capillary voltage 5 kV, nozzle voltage 1 kV, fragmentor voltage 420 V. The analysis was run in the positive mode with the reference masses of 121.050873 *m*/*z* and 922.009798 *m*/*z* and in the negative mode with the reference mass of

112.985587 *m*/*z* and 1033.988109 *m*/*z* for ion correction. The data acquisition was done in the rage of 100-1700 *m*/*z* with a scan rate of 1 s^{-1}.

Data analysis was performed with MassHunter software by Agilent Technologies. High resolution masses for **F1** and **F1*** were determined using the "Find by formula algorithm" with $C_{12}H_{13}NO_4$ and $C_{12}H_{12}O_5$ allowing for $[M+H]^+$ and $[M+Na]^+$ ions in the positive mode and in the negative mode within 10 ppm of the calculated *m*/*z* . Protein mass spectra deconvolution was done using the maximum entropy algorithm with a mass range of 5-30 kDa, a mass step of 1 Da, within a *m*/*z* range of 500-5,0000 a baseline factor of 8 and an isotope width of 25 Da.

3D Pharmacophore model generation: After preparation in MOE version 2014.09, the crystal structures 3ZZ6, 3ZZ7, 3ZZ8, 3ZZ9, 3ZZA, 3ZZB, 3ZZC and 3ZZD taken from the Protein data bank[45] (PDB) were loaded into the structure-based panel of LigandScout. For each structure a feature pattern representing the interactions of the protein-ligand complex was generated automatically and manually curated to ensure chemical reasonability. A shared feature pharmacophore was generated from the obtained feature patterns in the alignment panel of LigandScout. Validation was done by using by using biologically active ($k_{inact}/K_I \geq 100$ $M^{-1}s^{-1}$ or $K_i \leq 1$ μM) non-peptidic $3C^{pro}$ inhibitors reported by Reich *et al*., Webber *et al*. and Johnson *et al*., respectively.[30-32]

Protein-ligand docking: GOLD v 5.0.2 by the Cambridge Crystallographic Data Center (Cambridge, UK, Europe) was used for docking in the active site of the $3C^{pro}$. 3D conformations of the ligands were generated using CORINA.[46] The reacted state of the covalently binding ligands was generated through the reactor application by applying the appropriate SMIRKS patterns in respect to the warhead of the ligand. If the stereochemistry was known or a new stereo center was introduced through the covalent binding, all possible stereoisomers were

generated. As protein structure PDB entry 3ZZA for CVB3 and 3ZVG [47] for EV D68 were used after preparation in MOE version 2014.09. The binding-site was defined using a radius of 10 Å around the sulfur atom of Cys147. The docking was carried out using the PLP scoring function[48] with 25 GA runs per ligand in the most accurate mode without water molecules and default parameter settings.[48] Covalent docking was performed by constraining the sulfur atom in the ligand and C147 to have the same position with methanethiol as common substructure. Docking poses were analyzed and prioritized according the interactions represented in the 3D pharmacophore model in LigandScout.[26] Graphical representations were prepared either by using LigandScout version 4 or PyMOL Molecular Graphics System, Version 1.7.4 Schrödinger, LLC.

ABBREVIATIONS

CVB3, Coxsackievirus B3; EV D68, Enterovirus D68; $3C^{pro}$, 3C protease; GSH, Glutathione; PDB, Protein data bank; MALDI/TOF, Matrix assisted laser desorption ionization / time-of-flight;

KEY WORDS

3C Protease, 3D pharmacophore, Covalent fragments, Phenylthiomethyl ketone, Activity-based protein profiling, De novo design

ASSOCIATED CONTENT

Supporting information includes:

- Synthesis procedures, compound characterization, fragment selection from pharmacophore-based screening, biological activity against CVB3 and EV D68 $3C^{pro}$, sequence alignment for $3C^{pro}$ comparison, 3D pharmacophore validation (PDF)

- Molecular formula strings and activity values for the compounds (CSV)

AUTHOR INFORMATION

Corresponding Author

*G.W.: phone, +49 30 838 52686; gerhard.wolber@fu-berlin.de

Author Contributions

All authors have given approval to the final version of the manuscript.

Funding Sources

Notes

The authors declare no competing financial interest.

ACKNOWLEDGMENT

We thank the computing center of the FU Berlin (ZEDAT) for providing access to the compute cluster SOROBAN.

References

1. Roth, G. J.; Stanford, N.; Majerus, P. W. Acetylation of prostaglandin synthase by Aspirin. *Proc. Natl. Acad. Sci. U.S.A.* **1975,** *72*, 3073-3076.

2. Bryan, J. Carbapenems have stood the test of time so far but resistance is emerging. *Pharm. J.* **2014,** 292.

3. Mullin, R. Before the storm. *Chem. rev.* **2011,** 89.

4. Olbe, L.; Carlsson, E.; Lindberg, P. A proton-pump inhibitor expedition: the case histories of omeprazole and esomeprazole. *Nat. Rev. Drug Discov.* **2003,** *2*, 132-139.

5. Nakayama, S.; Atsumi, R.; Takakusa, H.; Kobayashi, Y.; Kurihara, A.; Nagai, Y.; Nakai, D.; Okazaki, O. A zone classification system for risk assessment of idiosyncratic drug toxicity using daily dose and covalent binding. *Drug Metab. Dispo.* **2009,** *37*, 1970-1977.

6. Singh, J.; Petter, R. C.; Baillie, T. A.; Whitty, A. The resurgence of covalent drugs. *Nat. rev. Drug Discov.* **2011,** *10*, 307-317.

7. Bauer, R. A. Covalent inhibitors in drug discovery: from accidental discoveries to avoided liabilities and designed therapies. *Drug Discov. Today* **2015**, *20*, 1061-1073.

8. Copeland, R. A. The dynamics of drug-target interactions: drug-target residence time and its impact on efficacy and safety. *Expert Opin. Drug Discov.* **2010**, *5*, 305-310.

9. Lammert, C.; Einarsson, S.; Saha, C.; Niklasson, A.; Bjornsson, E.; Chalasani, N. Relationship between daily dose of oral medications and idiosyncratic drug-induced liver injury: search for signals. *Hepatology* **2008,** *47*, 2003-2009.

10. Smith, A. J.; Zhang, X.; Leach, A. G.; Houk, K. N. Beyond picomolar affinities: quantitative aspects of noncovalent and covalent binding of drugs to proteins. *J. Med. Chem*. **2009**, *52*, 225-233.

11. Johnson, D. S.; Weerapana, E.; Cravatt, B. F. Strategies for discovering and derisking covalent, irreversible enzyme inhibitors. *Future Med. Chem.* **2010**, *2*, 949-964.

12. Miller, R. M.; Paavilainen, V. O.; Krishnan, S.; Serafimova, I. M.; Taunton, J. Electrophilic fragment-based design of reversible covalent kinase inhibitors. *J. Am. Chem. Soc.* **2013**, *135*, 5298-5301.

13. Erlanson, D. A.; Braisted, A. C.; Raphael, D. R.; Randal, M.; Stroud, R. M.; Gordon, E. M.; Wells, J. A. Site-directed ligand discovery. *Proc. Natl. Acad. Sci. U.S.A.* **2000**, *97*, 9367-9372.

14. Ostrem, J. M.; Peters, U.; Sos, M. L.; Wells, J. A.; Shokat, K. M. K-Ras(G12C) inhibitors allosterically control GTP affinity and effector interactions. *Nature* **2013,** 503.

15. Becker, D.; Kaczmarska, Z.; Arkona, C.; Schulz, R.; Tauber, C.; Wolber, G.; Hilgenfeld, R.; Coll, M.; Rademann, J. Irreversible inhibitors of the 3C protease of oxsackie virus through templated assembly of protein-binding fragments. *Nat. commun.* **2016,** *7*, 12761.

16. Cardoso, R.; Love, R.; Nilsson, C. L.; Bergqvist, S.; Nowlin, D.; Yan, J. L.; Liu, K. K. C.; Zhu, J.; Chen, P.; Deng, Y. L.; Dyson, H. J.; Greig, M. J.; Brooun, A. Identification of Cys255 in HIF-1 alpha as a novel site for development of covalent inhibitors of HIF-1 alpha/ARNT PasB domain protein-protein interaction. *Protein Sci.* **2012**, *21*, 1885-1896.

17. Kathman, S. G.; Xu, Z.; Statsyuk, A. V. A fragment-based method to discover irreversible covalent inhibitors of cysteine proteases. *J. Med. Chem.* **2014**, *57*, 4969-4974.

18. Jaegle, M.; Wong, E. L.; Tauber, C.; Nawrotzky, E.; Arkona, C.; Rademann, J. Protein-templated fragment ligations-from molecular recognition to drug discovery. *Angew. Chem. Int. Ed.* **2017**, *56*, 7358-7378.

19. Wong, A. H.; Lau, C. S.; Cheng, P. K.; Ng, A. Y.; Lim, W. W. Coxsackievirus B3-associated aseptic meningitis: an emerging infection in Hong Kong. *J. Med. Virol* **2011**, *83*, 483-489.

20. Nakamura, H.; Yamamoto, T.; Yamamura, T.; Nakao, F.; Umemoto, S.; Shintaku, T.; Yamaguchi, K.; Liu, P.; Matsuzaki, M. Repetitive coxsackievirus infection induces cardiac dilatation in post-myocarditic mice. *Circ. J.* **1999**, *63*, 794-802.

21. Richer, M. J.; Horwitz, M. S. Coxsackievirus infection as an environmental factor in the etiology of type 1 diabetes. *Autoimmun. Rev.* **2009**, *8*, 611-615.

22. Mantri, S.; Shah, B. B. Enterovirus causes rapidly progressive dementia in a 28-year-old immunosuppressed woman. *J. Neurovirol.* **2016**, *22*, 538-540.

23. Wang, Q. M. Protease inhibitors as potential antiviral agents for the treatment of picornaviral infections. *Prog Drug Res.* **2001**, Spec No, 229-253.

24. Zhang, X. N.; Song, Z. G.; Qin, B. Y.; Zhang, X. L.; Chen, L. X.; Hu, Y. W.; Yuan, Z. H. Rupintrivir is a promising candidate for treating severe cases of enterovirus-71 infection: evaluation of antiviral efficacy in a murine infection model. *Antivir. Res.* **2013,** *97*, 264-269.

25. Patick, A. K.; Brothers, M. A.; Maldonado, F.; Binford, S.; Maldonado, O.; Fuhrman, S.; Petersen, A.; Smith, G. J. In vitro antiviral activity and single-dose pharmacokinetics in humans of a novel, orally bioavailable inhibitor of human rhinovirus 3C protease. *Antimicrob. Agents Ch.* **2005**, *49*, 2267-2275.

26. Wolber, G.; Langer, T. LigandScout: 3-D pharmacophores derived from protein-bound ligands and their use as virtual screening filters. *J. Chem. Inf. Model.* **2005**, *45*, 160-169.

27. Otto, H. H.; Schirmeister, T. Cysteine proteases and their inhibitors. *Chem. Rev.* **1997**, *97*, 133-172.

28. Powers, J. C.; Asgian, J. L.; Ekici, O. D.; James, K. E. Irreversible inhibitors of serine, cysteine, and threonine proteases. *Chem. Rev.* **2002**, *102*, 4639-4750.

29. Shannon, D. A.; Weerapana, E. Covalent protein modification: the current landscape of residue-specific electrophiles. *Curr. Opin. Chem. Biol.* **2015**, *24*, 18-26.

30. Reich, S. H.; Johnson, T.; Wallace, M. B.; Kephart, S. E.; Fuhrman, S. A.; Worland, S. T.; Matthews, D. A.; Hendrickson, T. F.; Chan, F.; Meador, J.; Ferre, R. A.; Brown, E. L.; DeLisle, D. M.; Patick, A. K.; Binford, S. L.; Ford, C. E. Substituted benzamide inhibitors of human rhinovirus 3C protease: structure-based design, synthesis, and biological evaluation. *J. Med. Chem.* **2000**, *43*, 1670-1683.

31. Webber, S. E.; Tikhe, J.; Worland, S. T.; Fuhrman, S. A.; Hendrickson, T. F.; Matthews, D. A.; Love, R. A.; Patick, A. K.; Meador, J. W.; Ferre, R. A.; Brown, E. L.; DeLisle, D. M.; Ford, C. E.; Binford, S. L. Design, synthesis, and evaluation of nonpeptidic inhibitors of human rhinovirus 3C protease. *J. Med. Chem.* **1996**, *39*, 5072-5082.

32. Johnson, T. O.; Hua, Y.; Luu, H. T.; Brown, E. L.; Chan, F.; Chu, S. S.; Dragovich, P. S.; Eastman, B. W.; Ferre, R. A.; Fuhrman, S. A.; Hendrickson, T. F.; Maldonado, F. C.; Matthews, D. A.; Meador, J. W.; Patick, A. K.; Reich, S. H.; Skalitzky, D. J.; Worland, S. T.; Yang, M.; Zalman, L. S. Structure-based design of a parallel synthetic array directed toward the discovery of irreversible inhibitors of human rhinovirus 3C protease. *J. Med. Chem.* **2002**, *45*, 2016-2023.

33. Jhoti, H.; Williams, G.; Rees, D. C.; Murray, C. W. The 'rule of three' for fragment-based drug discovery: where are we now? *Nat. Rev. Drug Discov.* **2013**, *12*, 644-645.

34. Baell, J. B.; Holloway, G. A. New substructure filters for removal of pan assay interference compounds (PAINS) from screening libraries and for their exclusion in bioassays. *J. Med. Chem*. **2010**, *53*, 2719-2740.

35. Vodolazhenko, M. A.; Gorobets, N. Y.; Yermolayev, S. A.; Musatov, V. V.; Chebanov, V. A.; Desenko, S. M. Application of stable fused dienolates for diversity oriented synthesis of 2,5-dioxo-5,6,7,8-tetrahydro-2H-chromene-3-carboxamides. *Rsc. Adv*. **2012**, *2*, 1106-1111.

36. Dragovich, P. S.; Webber, S. E.; Babine, R. E.; Fuhrman, S. A.; Patick, A. K.; Matthews, D. A.; Reich, S. H.; Marakovits, J. T.; Prins, T. J.; Zhou, R.; Tikhe, J.; Littlefield, E. S.; Bleckman, T. M.; Wallace, M. B.; Little, T. L.; Ford, C. E.; Meador, J. W.; Ferre, R. A.; Brown, E. L.; Binford, S. L.; DeLisle, D. M.; Worland, S. T. Structure-based design, synthesis, and biological evaluation of irreversible human rhinovirus 3C protease inhibitors. 2. peptide structure-activity studies. *J. Med. Chem.* **1998**, *41*, 2819-2834.

37. Schneider, G.; Neidhart, W.; Giller, T.; Schmid, G. "Scaffold-hopping" by topological pharmacophore search: a contribution to virtual screening. *Angew. Chem*. **1999**, *38*, 2894-2896.

38. Hu, Y.; Stumpfe, D.; Bajorath, J. Advancing the activity cliff concept. *F1000Res.* **2013,** *2*, 199.

39. Perez, D. I.; Palomo, V.; Perez, C.; Gil, C.; Dans, P. D.; Luque, F. J.; Conde, S.; Martinez, A. Switching reversibility to irreversibility in glycogen synthase kinase 3 inhibitors: clues for specific design of new compounds. *J. Med. Chem.* **2011,** *54*, 4042-4056.

40. WDI, Derwent World Drug Index, Release 2005, Derwent Information Ltd., London, UK

41. Lisurek, M.; Rupp, B.; Wichard, J.; Neuenschwander, M.; von Kries, J. P.; Frank, R.; Rademann, J.; Kuhne, R. Design of chemical libraries with potentially bioactive molecules applying a maximum common substructure concept. *Molec. Divers.* **2010**, *14*, 401-408.

42. Berthold, M. R.; Cebron, N.; Dill, F.; Gabriel, T. R.; Kötter, T.; Meinl, T.; Ohl, P.; Sieb, S.; Thiel, K.; Wiswedel, B. KNIME: The (K)onstanz (I)nformation (M)iner. In *Studies in Classification, Data Analysis, and Knowledge Organization (GfKL 2007)*, Springer: **2007**.

43. RDKit: Open-source cheminformatics; http://www.rdkit.org. *accessed December 1, 2017.*

44. Davis, B. J.; Erlanson, D. A. Learning from our mistakes: the 'unknown knowns' in fragment screening. *Bioorg. Med. Chem. Lett.* **2013**, *23*, 2844-2852.

45. Berman, H. M.; Westbrook, J.; Feng, Z.; Gilliland, G.; Bhat, T. N.; Weissig, H.; Shindyalov, I. N.; Bourne, P. E. The protein data bank. *Nucleic Acids Res.* **2000**, *28*, 235-242.

46. Sadowski, J.; Gasteiger, J.; Klebe, G. Comparison of automatic 3-dimensional model builders using 639 X-ray structures. *J. Chem. Inf. Comp. Sci.* **1994**, *34*, 1000-1008.

47. Tan, J.; George, S.; Kusov, Y.; Perbandt, M.; Anemuller, S.; Mesters, J. R.; Norder, H.; Coutard, B.; Lacroix, C.; Leyssen, P.; Neyts, J.; Hilgenfeld, R. 3C protease of enterovirus 68: structure-based design of Michael acceptor inhibitors and their broad-spectrum antiviral effects against picornaviruses. *J. Virol.* **2013,** *87*, 4339-4351.

48. Korb, O.; Stutzle, T.; Exner, T. E. Empirical scoring functions for advanced protein-ligand Docking with PLANTS. *J. Chem. Inf. Model.* **2009,** *49*, 84-96.

Table of content figure

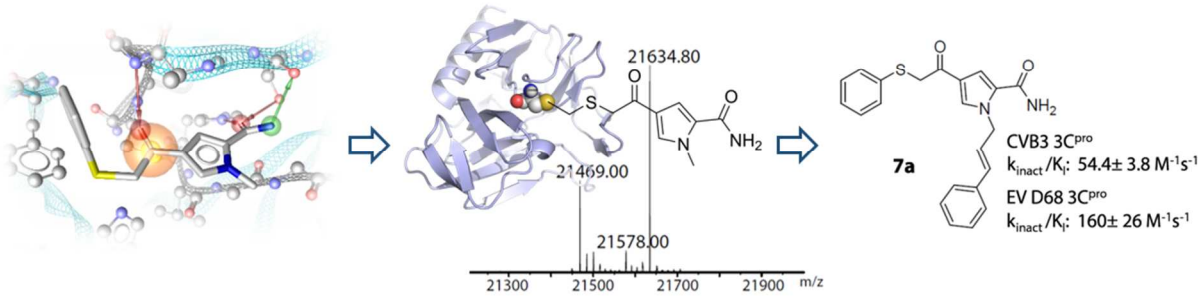

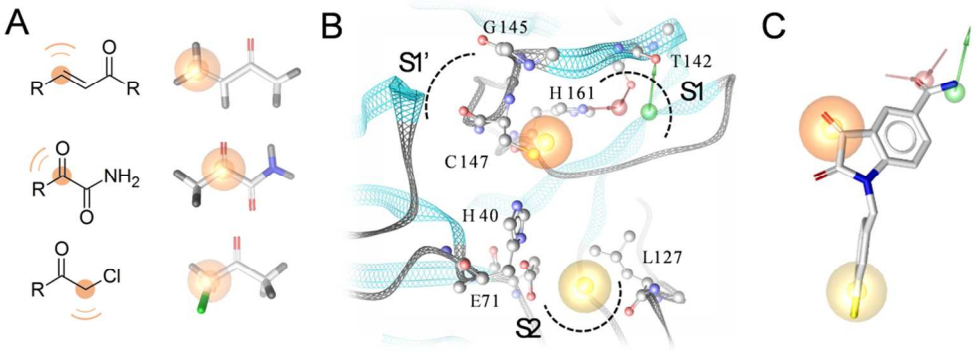

Figure 1

101x37mm (300 x 300 DPI)

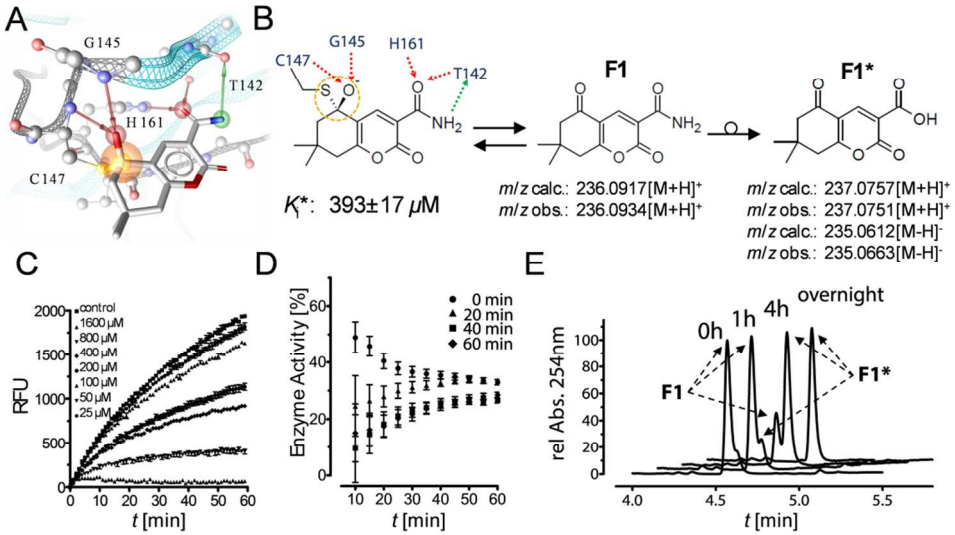

Figure 2

101x55mm (300 x 300 DPI)

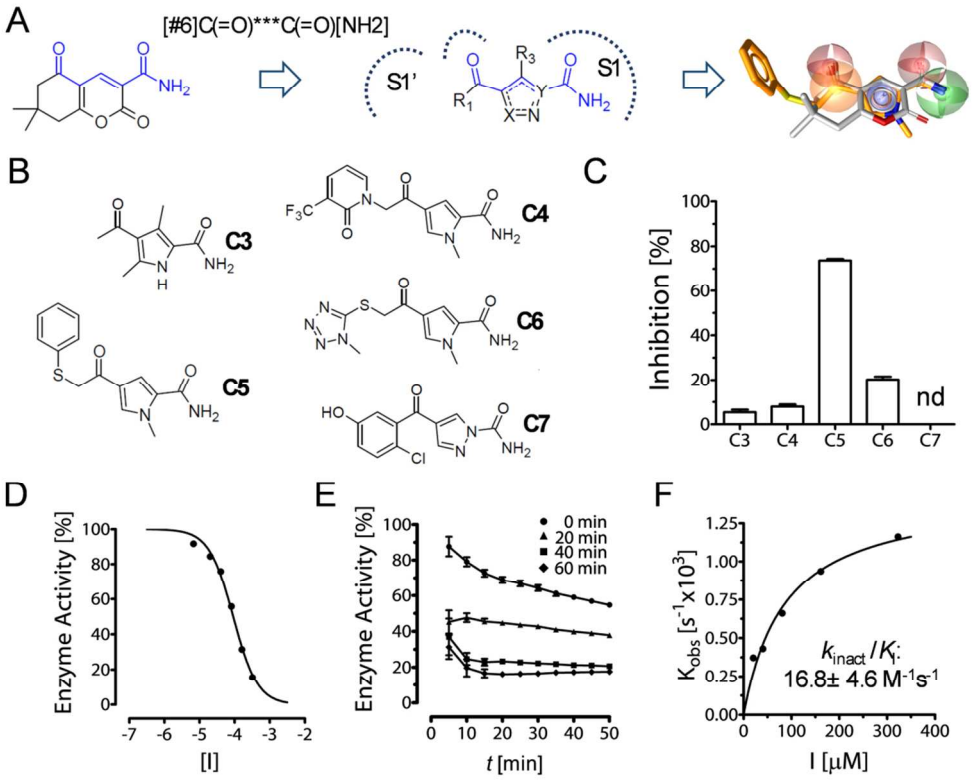

Figure 3

101x80mm (300 x 300 DPI)

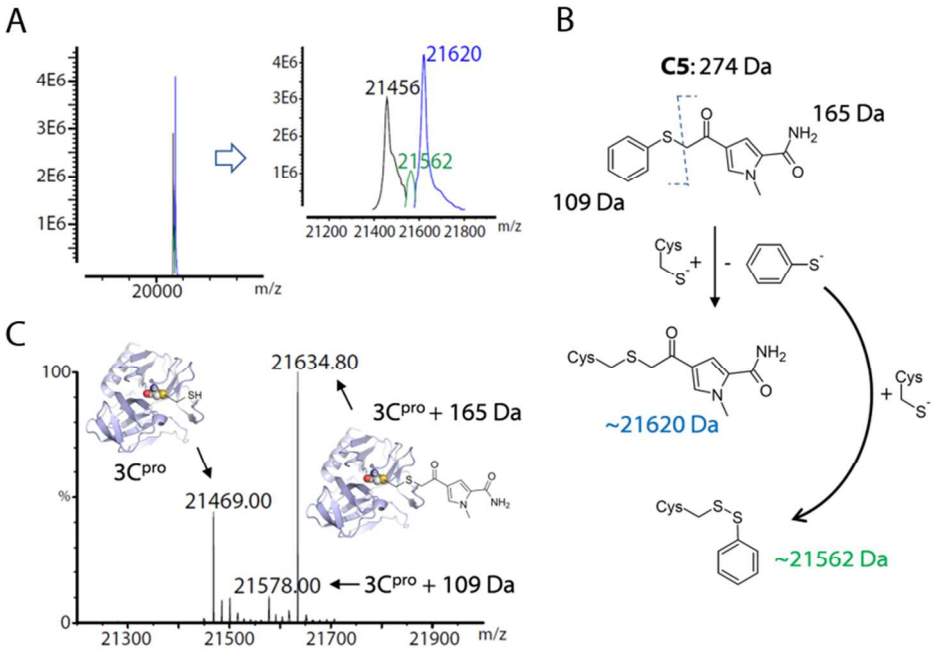

Figure 4

80x53mm (300 x 300 DPI)

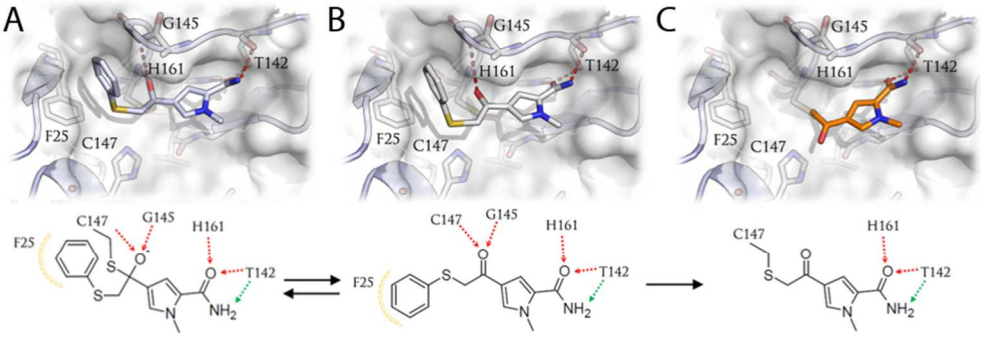

Figure 5

80x28mm (300 x 300 DPI)

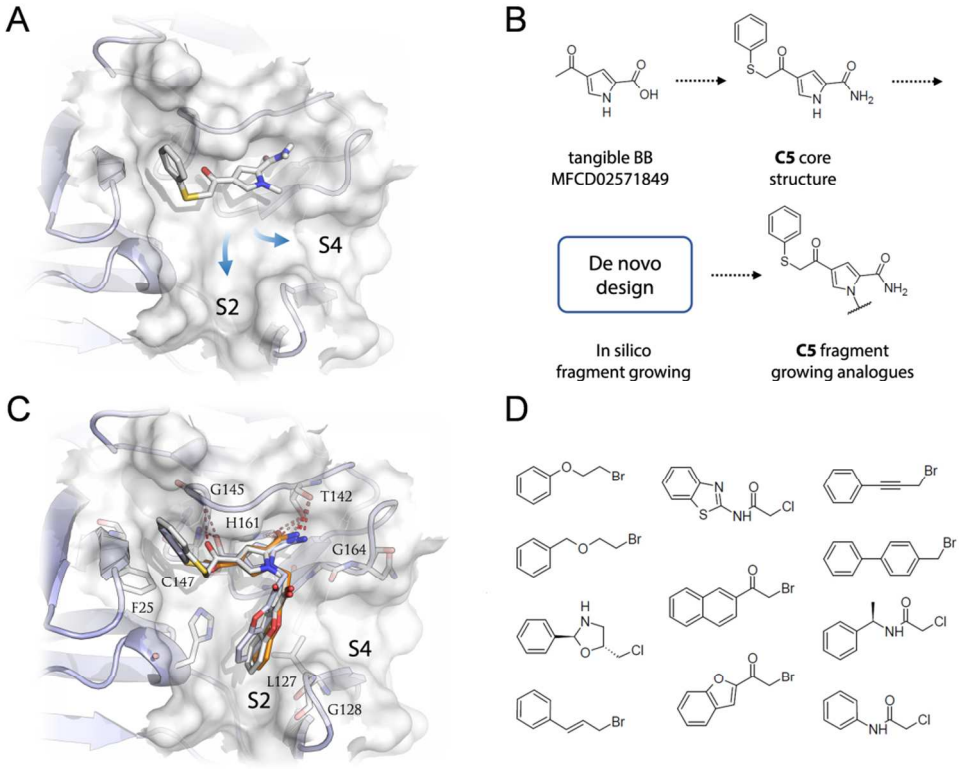

Figure 6

101x79mm (300 x 300 DPI)

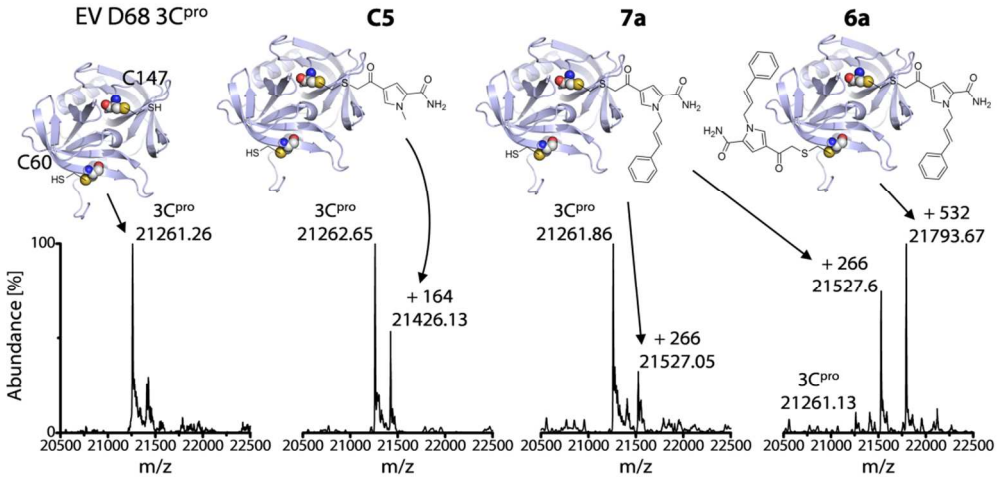

Figure 7

101x48mm (300 x 300 DPI)

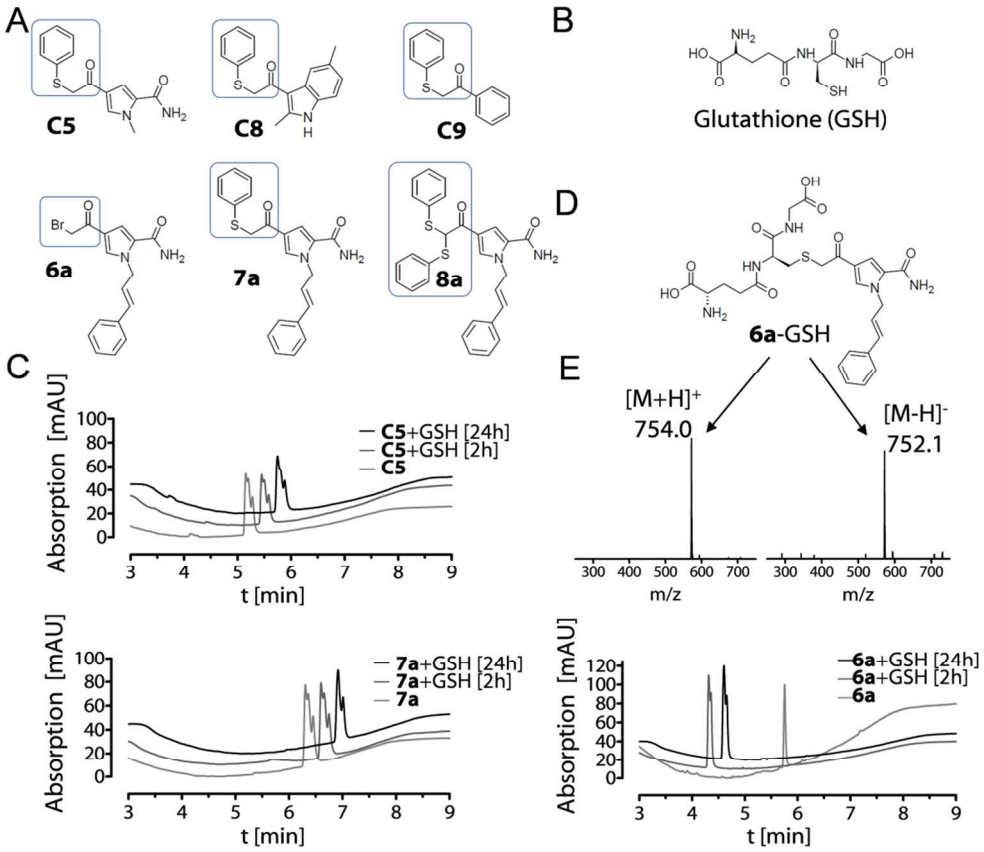

Figure 8

101x87mm (300 x 300 DPI)

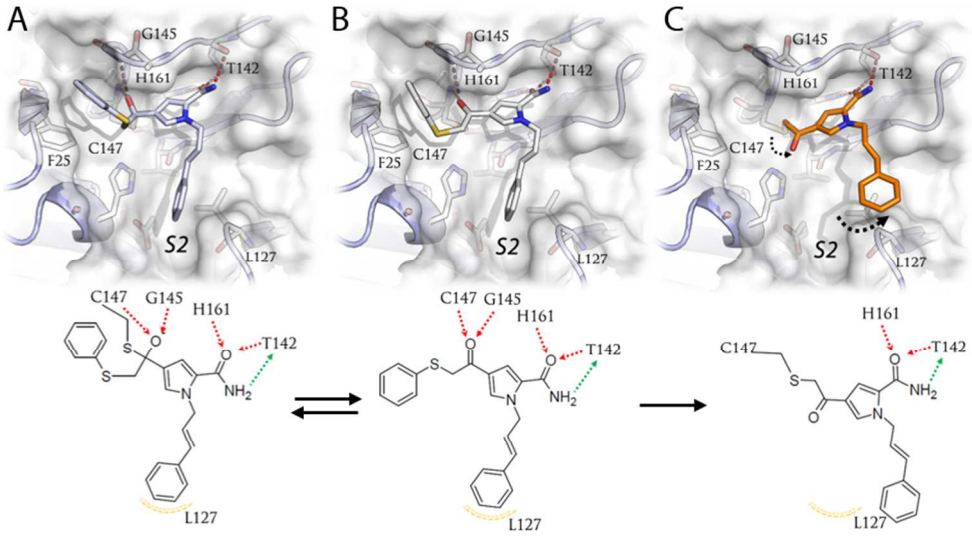

Figure 9

81x44mm (300 x 300 DPI)

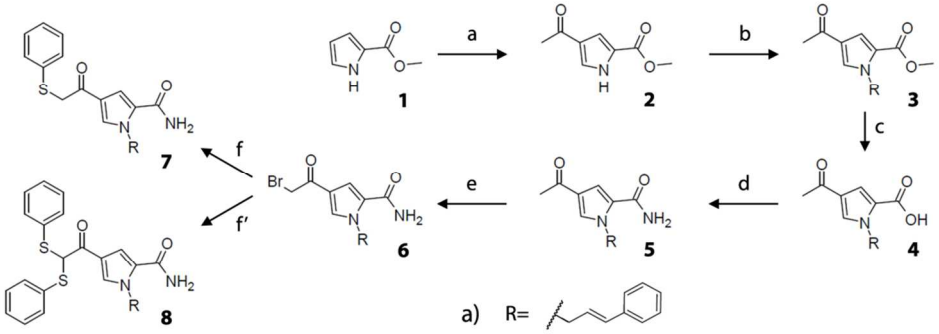

Scheme 1

101x35mm (300 x 300 DPI)

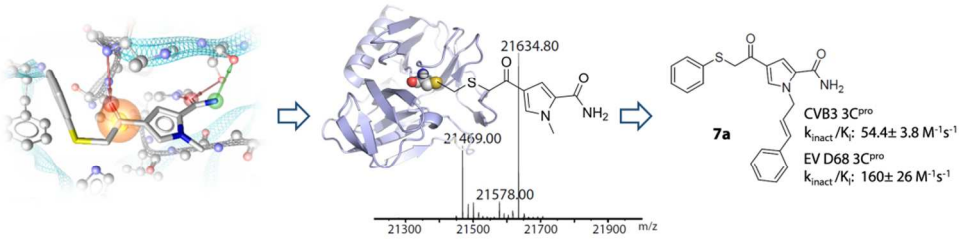

Table of contents graphics

101x26mm (300 x 300 DPI)